Regional challenges concerning derivation of suspended particulate matter concentration and water turbidity from water reflectance. A case study in the western Black Sea

Sorin Constantin, Ioan-Daniel Șerban, David Doxaran, Fabrizio d'Ortenzio

Estuarine, Coastal and Shelf Science 305 (2024) 108871

Contents lists available at ScienceDirect

Estuarine, Coastal and Shelf Science

journal homepage: www.elsevier.com/locate/ecss

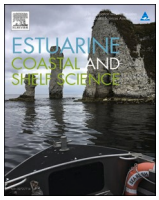

Regional challenges concerning derivation of suspended particulate matter concentration and water turbidity from water reflectance. A case study in the western Black Sea

Sorin Constantin [a,b,*], Ioan-Daniel Șerban [a,b], David Doxaran [c], Fabrizio D'Ortenzio [c]

[a] University of Bucharest, 050663, Bucharest, Romania
[b] Terrasigna, 020581, Bucharest, Romania
[c] Laboratoire d'Océanographie de Villefranche UMR 7093, CNRS Sorbonne Université, 06230 Villefranche-sur-Mer, France

ARTICLE INFO

Keywords:
Suspended particulate matter
Water turbidity
Water-leaving reflectance
Black sea
Sentinel-3
OLCI

ABSTRACT

Assessment of water quality indicators, such as Suspended Particulate Matter (SPM) concentration and water turbidity (TUR) is essential for marine ecosystems health evaluations. This work focuses on the estimation of these two variables from water-leaving reflectance measurements, either derived from in-situ observations or satellite data, for the western Black Sea basin. The regional characteristics of the water optically active constituents can have important impact on the quality of such estimations if not properly accounted for. We test several existing inversion algorithms and quantify their accuracy. New, regionally adapted methods are then proposed, together with a new formulation for a multi-conditional switching mechanism. Calibration of these models is performed based on SPM and TUR in-situ measurements. It is shown that the improvements achieved through regional adaptation can be significant. Application of these algorithms to Sentinel-3 OLCI satellite data reveals the consistency of the proposed methodology. Also, it shows the degree of uncertainty if improper formulations are used, with major impact on the absolute values of retrieved SPM or TUR.

1. Introduction

Suspended Particulate Matter (SPM) concentration and water turbidity (TUR) are two key water quality indicators that can be successfully retrieved from satellite optical data and are important for the evaluation of ecosystems health status (Bilotta and Brazier, 2008). The use of satellite remote sensing information for studies concerning water quality has witnessed significant advances in the last decades. Recently, the increased number of dedicated and/or adaptable satellite sensors led to an exponential availability of datasets for such applications (Pahlevan et al., 2021 and references therein). Nevertheless, while important progress has been made also in the realm of dedicated algorithms for the processing of satellite data recorded over open ocean and coastal waters, there are still knowledge gaps that need to be filled. This is especially true in areas characterized by complex environmental conditions, where the water column optical properties are influenced by a mixture of colored constituents, with diverse composition patterns and a broad range of particle-size distributions and shapes. The relation between SPM and optical properties (apparent or inherent) covary lightly with changes in the particulate composition (Stramski et al., 2023). Shifts from mineral to organic dominated particles (providing there are no changes in terms of shape and size) will have little influence on this relationship. On the other hand, changes in particles dimensions, which affect the volume scattering function, will largely contribute to regional peculiarities when trying to determine SPM from optical data (Nechad et al., 2010). Since TUR is an optical property, closely related to the back (or side) scattering coefficient (and thus to the water reflectance), the conversion from optical measurements is less influenced by changes in particles morphology (Dogliotti et al., 2015).

Numerous studies have tackled the estimation of SPM and TUR based on remote sensing data (e.g., Doxaran et al., 2002; Ody et al., 2016; Novoa et al., 2017). Most of these endeavors are focused on regional applicability of such inversion schemes. Very few adventured into developing algorithms that are generally valid, meaning those that have the potential to be applicable on a broad scale of water optical types, while obtaining similar accuracy in each situation (Nechad et al., 2009, 2010; Dogliotti et al., 2015; Han et al., 2016; Yu et al., 2019; Balasubramanian et al., 2020; Tavora et al., 2020; Wei et al., 2021).

* Corresponding author. University of Bucharest, 050663, Bucharest, Romania.
E-mail address: sorin.constantin@icub.unibuc.ro (S. Constantin).

https://doi.org/10.1016/j.ecss.2024.108871
Received 18 December 2023; Received in revised form 3 July 2024; Accepted 4 July 2024
Available online 5 July 2024

For the Black Sea area, one of the first attempts to use satellite reflectance for the estimation of SPM was based on Landsat MSS (Multispectral Scanner) and TM (Thematic Mapper) data from the green and red parts of the electromagnetic spectrum (Brăescu et al., 1997). While no empirical algorithm was provided, the study showed good correlation between SPM and water radiance in the aforementioned spectral bands. Kukushkin and Suslin (2020) have analyzed the relation between in-situ SPM measurements and satellite derived inherent optical properties (scattering and absorption coefficients) and chlorophyll-a concentration, for the eastern and western deep-sea parts. They show good agreement between these variables and highlight the potential use of satellite data to monitor SPM. However, they do not tackle the relationship between SPM and water-leaving reflectance. Nazirova et al. (2021), focused their research on a small area in front of Mzymta River, in the western part of the Black Sea. They investigated the possibility to derive SPM and TUR using reflectance data from Sentinel-2 and Landsat 8 satellites, based on existing inversion algorithms (without local calibration). Due to regional characteristics, the same drawbacks as shown in this current study and presented hereafter were found. In terms of turbidity mapping, Güttler et al. (2013) used MERIS (Medium Resolution Imaging Spectrometer) data to evaluate the turbidity dynamics in the Romanian coastal area, with turbidity computed as a factor of non-algal (mineral) suspended particulate matter and chlorophyll concentrations. A dedicated regional empirical algorithm was also proposed using match-ups between in-situ turbidity measurements and water reflectance values derived from MODIS (Moderate Resolution Imaging Spectroradiometer) satellite data (Constantin et al., 2016). More recent endeavours to augment the usage and the quality of Earth Observation products for the Black Sea region have been undertaken in the frame of European Space Agency's regional initiatives. In this regard, concerning ocean colour activities, three parameters of interest were targeted, in order to improve the potential datasets by developing new processing procedures and biogeochemical variables estimation: chlorophyll-a and SPM concentrations and water turbidity (Grégoire et al., 2023).

The main objectives of the current study are: i) to test existing approaches for estimation of SPM and TUR based on water reflectance data and asses their performance for the western Black Sea basin and ii) calibrate and tune regionally adapted algorithms that can increase the accuracy of the predicted SPM and TUR values. The study area is restricted only to the western part of the Black Sea due to the fact that in-situ samples were available only for this region. A complementary goal is to investigate the potential of Sentinel-3 OLCI (Ocean and Land Colour Instrument) satellite products to characterize the SPM concentration and water turbidity in the area of interest. Thus, existing general algorithms are tested and new formulations are provided for a more accurate estimation of these two essential water quality parameters. This work has the potential for an operational application, since it can contribute to the provision of enhanced products based on water-leaving reflectance data coming from standard marine Level 2 OLCI products. However, validation of new parameterizations with independent in-situ data is first required. Better definition of algorithms for SPM and TUR estimation using water reflectance can contribute to a finer understanding of the physical and biological processes governing the local marine environment and can offer improved tools for studies in these directions (e.g., Karageorgis et al., 2009; Stanev and Kandilarov, 2012; Preoteasa et al., 2016; Constantin et al., 2017; Kubryakov et al., 2018; Zăinescu et al., 2019; Constantinescu et al., 2023).

In this paper we show that general inversion algorithms for SPM and TUR retrieval, while performing well overall, still need regional adaptation and adjustments in specific scenarios. And that the usage of multi-conditional algorithms can benefit optically complex waters. This is the case of the Black Sea western basin, highly influenced by important sediment inputs from river discharge (Stanev and Kandilarov, 2012), intense algal blooms (Sorokin, 1983) and also high values of colored dissolved organic matter (Ducklow et al., 2007; Margolin et al., 2018).

2. Methodology

2.1. Study area, data sources and statistical analysis

The analyses in this study are based on match-ups between water-leaving reflectance values (ρ_w, dimensionless) and field measurements of two biogeochemical parameters of interest: water turbidity (TUR, in NTU) and the Suspended Particulate Matter (SPM, in g m^{-3}) concentration, in the western Black Sea region. In order to build this dataset, two distinct sources of information were used.

The first refers to the compilation of global bio-optical in-situ data provided by Valente et al. (2022). The data brings together 27 different sources. The observations covering the Black Sea area are represented by the MERIS Match-up In Situ Database (MERMAID). Therefore, the subset used hereafter will be denoted MERM. The dataset gives access to match-ups (concomitant sampling) between in-situ radiometric measurements (above-water remote sensing reflectance – R_{rs}, in sr^{-1}) and SPM concentrations (in g m^{-3}) (Table 2). No TUR measurements are available for this dataset.

The second data source corresponds to field campaigns organized in the proximity of the Danube Delta coastal area (dataset hereafter referred to as DP, from "Danube Plume"). For this particular case, in-situ SPM and TUR measurements were matched with ρ_w values extracted from concurrent Sentinel-3 OLCI Level 2 products (a total of 61 match-ups, out of which 47 with a time difference of less than 2 h, 7 between 2 and 3 h and 6 between 4 and 5 h). Overall, the final combined dataset used hereafter contains both in-situ and satellite derived radiometric measurements (a total of 88 match-ups; 74 for SPM and 55 for TUR; see Table 2).

The geographical locations of the match-ups cover a broad area of the western basin of the Black Sea (Fig. 1). Most of them overlap the continental shelf. While the MERM samples are distributed over this entire region, the DP match-ups are grouped in front of the mouth of the southern Danube's branch - Sfântu Gheorghe. MERM data were collected during 5 days in 2011: July 1, 3, 9, 11 and 12. DP samples and concomitant match-ups with satellite-derived ρ_w values are available for the following dates: March 18, 2019; June 23, 2019; August 7, 2019; November 2, 2020; April 9, 2021 and October 22, 2021. For August 7, 2019, two OLCI images were available, since both platforms, Sentinel-3A and Sentinel-3B passed over the area of interest. The time difference between the two acquisitions is 40 min. Match-ups were computed for both images.

Several statistical indicators (Table 1) are hereafter used to characterize the goodness of fit for regression models. For the purpose of formulating relations between ρ_w and SPM or TUR, the model-I regression approach was used. For assessing the differences between model-derived and measured values, the model-II regression was chosen (Bellacicco et al., 2019). Given the restricted number of available match-ups, the entire dataset was used for calibration. Therefore, the statistics that show the consistency between observed and predicted SPM or TUR are computed based on the same in-situ samples that were used for algorithm-development purposes. Independent data for validation activities would be valuable. However, a very limited number of measurements is available for this region of interest. Also, the current study is focused only on algorithm testing and calibration.

A bootstrap approach was used in order to compare the regional calibrated coefficients (for the new proposed parameterizations, which are based on all original match-ups) with random sampling results. This step involves randomly selecting from the input dataset and fitting a regression model to each scenario. Each bootstrap run is based on 10000 replications. The median values of coefficients for all replications are finally considered. In the absence of independent measurements for validation, this method helps to partly and indirectly assess how much overfitting of the algorithms to the calibration data is present, depending on the magnitude of deviations from original coefficients.

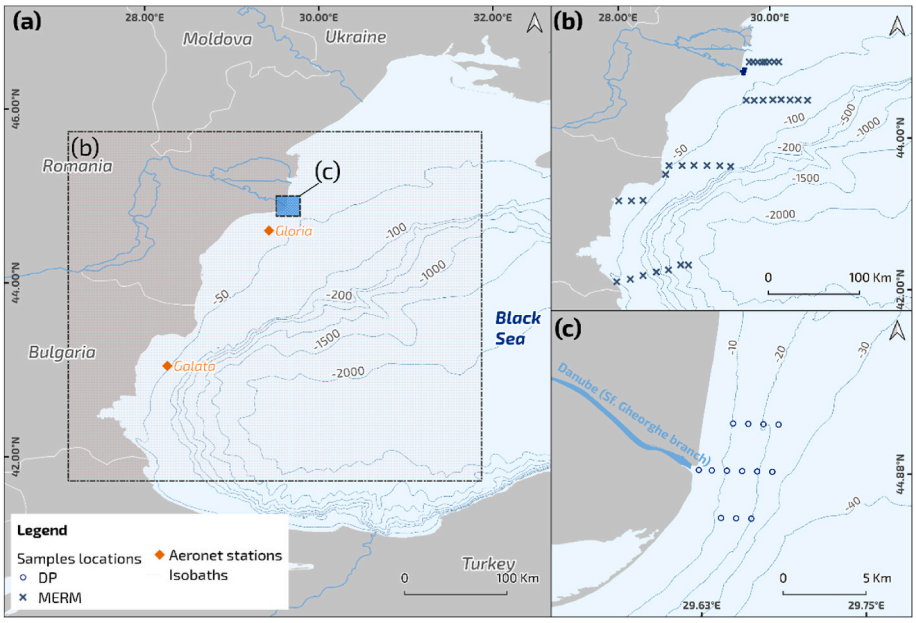

Fig. 1. Location of match-up samples between Suspended Particulate Matter (SPM) concentrations or water turbidity (TUR) and water-leaving reflectance (ρ_w).

Table 1
Statistical indicators used in characterization of the goodness-of-fit of algorithmic formulas, where n is the number of samples, P_i are predicted values, O_i are the observed values and *med* stands for median (for n samples, with an increment of $i = 1$).

Name and notation	Equation / Description
Correlation Coefficient (R)	$R = \frac{\sum_{i=1}^{n}(P_i - \overline{P})(O_i - \overline{O})}{\sqrt{\sum_{i=1}^{n}(P_i - \overline{P})^2}\sqrt{\sum_{i=1}^{n}(O_i - \overline{O})^2}}$
Standard deviation (σ)	$\sigma = \sqrt{\frac{\sum_{i=1}^{n}(P_i - \overline{P})^2}{n}}$
Root Mean Square Difference ($RMSD$)	$RMSD = \left[\frac{1}{N}\sum_{i=1}^{n}(P_i - O_i)^2\right]^{1/2}$
Median Bias (MdB)	$MdB = med(P_i - O_i)$
Median Ratio (MdR)	$MdR = med\left(\frac{P_i}{O_i}\right)$
Median Absolute Percentage Difference ($MdAPD$)	$MdAPD = 100\ med\left(\frac{\lvert P_i - O_i\rvert}{O_i}\right)$
Slope (S) and intercept (I)	Slope and intercept of a linear regression (either model-I or model-II)

Table 2
Summary of statistics for the SPM and TUR samples used for algorithms testing and definition; n is the number of available observations; selection was performed taking into consideration all samples that had at least one match-up with one wavelength from the following three: 560 nm, 665 nm or 865 nm.

Datasets	n	*Minimum*	*Maximum*	*Mean*	*Median*
SPM – all (g m^{-3})	74	0.34	81.33	8.82	3.96
SPM - DP (g m^{-3})	41	2.00	81.33	14.98	10.73
SPM - MERM (g m^{-3})	33	0.34	4.25	1.16	0.61
TUR - DP (NTU)	55	2.39	74.87	17.69	13.40

2.2. Suspended particulate matter concentration and water turbidity in-situ measurements

For the DP samples, water turbidity measurements were collected using a handheld turbidimeter (Hach 2100Q), with side scattering of light at 90°, a measurement range between 0 and 1000 NTU (Nephelometric Turbidity Units) and an accuracy of ±2% of reading plus stray (which is ≤ 0.02 NTU). Calibration of the instrument was performed before each field campaign, following the procedure provided by the manufacturer. Water samples were collected from the surface layer (approximately 5–20 cm depth). The auto-range function of the instrument was used, which provides mean values for multiple determinations within a period of couple of seconds. Moreover, triplicate measurements were systematically performed for each water sample, as recommended by Dogliotti et al. (2015). The associated absolute mean coefficient of variation for these triplicates is ±3.96% ($n = 60$).

The in-situ determinations of the mass concentration of dried Suspended Particulate Matter (SPM) per unit volume of water (in units of g m^{-3}) were performed using a standard gravimetric method, for the DP data. Water samples were filtered using pre-dried and pre-weighted Whatman GF/F glass-fiber filters (47 mm diameter) with a 0.7 μm pore size. The dry mass of particles was determined using a Kern ADB 200-4 analytical balance with a 0.1 mg precision. The loading of each filter was computed based on the recommendations from Neukermans et al. (2012), which provide look-up tables for determination of the optimal volume of water to be filtered based on the values of TUR. Unlike the case of TUR measurements, triplicates were available only for 10 out of the total 74 samples. The absolute mean coefficient of variation for these triplicates of SPM determinations is ±7.88% ($n = 10$). Despite the reduced geographical coverage of the DP samples, a broad range of SPM and TUR is available (Table 2), given the multiple organized campaigns overlapping various environmental conditions.

The relation between SPM and TUR, for the DP set, is given by the following linear equation:

$$\mathrm{SPM} = 0.9278\ \mathrm{TUR}, \text{with } n = 45 \text{ and } R = 0.99 \quad (1)$$

or by the second order polynomial fit, which provides slightly better approximations for higher values:

$$\mathrm{SPM} = 0.73205\ \mathrm{TUR} + 0.00477\ \mathrm{TUR}^2, \text{with } n = 45 \text{ and } R = 0.99 \quad (2)$$

These relations are similar to other studies, like Novoa et al. (2017), where the value of the slope for a linear fit (as in eq. (1)) is 0.88, or between 0.8 and 0.9 (Nechad et al., 2009). For the western Black Sea area (Mzymta River plume), Nazirova et al. (2021) found a value of 0.84. Nevertheless, other authors have reported different coefficients, for diverse areas, with the same slope value reaching as high as 1.85 (Gohin, 2011) or 1.49 (with a non-zero intercept) (Doxaran, 2002). Jafar-Sidik et al. (2017) showed, for the Liverpool Bay, that the ratio

between SPM and TUR can have also seasonal variations (between 0.91 and 1.46), depending on the type of particles dominant in various months of the year. All these differences partly come from the different turbidity sensors used in each study, but also highlight the complexity of particles assemblages found in natural waters and the need to derive adapted algorithms for remote sensing applications.

MERM SPM data (denoted TSM by the authors - Total Suspended Matter) have been measured during BioOptEuroFleets campaigns, undertaken by the Joint Research Center (JCR) of the European Commission (Barker, 2013b). The procedure is similar to the one used for the DP samples. It implies the usage of GF filters with 0.7 μm pore size (Zibordi et al., 2002). The only difference is represented by the storage of filters at −18 °C after filtration, for subsequent laboratory analysis, while for DP samples the entire process was performed continuously, without the need for storage between different stages.

During the total eleven days for which in-situ measurements are available, various hydrological conditions on the Danube River were observed. If water level measurements at Tulcea station, located at the delta apex, are to be considered, the following quantile distribution of daily values for a long period of time (2000–2022) is observed: 5 cm, 107 cm, 172 cm, 247 cm and 439 cm (representing minimum, 25th percentile, median, 75th percentile and maximum values). For the five days when SPM MERM measurements were taken, the following Danube water levels were registered: 116 cm, 125 cm, 127 cm, 134 cm and 135 cm; for the six days associated with the DP dataset: 72 cm, 93 cm, 191 cm, 204 cm, 217 cm and 364 cm. The broad range of SPM and TUR values, collected during diverse Danube water level scenarios, provides evidence that the input datasets are representative for multiple cases in terms of potential particle characteristics and other optically active constituents with riverine origin. Thus, the potential composition, size and shape of these particles, which dictate the relation between SPM or TUR and ρ_w and which are directly affected by the river outputs, should be well accounted for.

2.3. Water-leaving reflectance measurements

For the purpose of the current study, the water-leaving reflectance (ρ_w) is defined as the ratio between the irradiance in all the upward directions, or upwelling irradiance at a specific wavelength (E_u, in W m^{-2} nm^{-1}) and the irradiance in the downward direction, or the downwelling irradiance (E_d, in W m^{-2} nm^{-1}) at the same wavelength (eq. (3)). Both E_u and E_d are computed or measured just above the sea surface.

$$\rho_w(\lambda) = \frac{E_u(\lambda)}{E_d(\lambda)} \quad (3)$$

The ρ_w measurements to be matched with the SPM and TUR have two different origins: satellite derived, for the DP dataset, and in-situ acquired, for the MERM series. For the first case, extractions were performed using Sentinel-3 OLCI standard Level 2 products, which were acquired through EUMETSAT Data Center facility. All datasets before February 2021 belong to Collection 2, while the newer ones are processed under the Collection 3 umbrella (EUMETSAT, 2021). While reprocessing of the entire archive is foreseen, this was not performed by the time this study was written. Reasons for selecting OLCI (https://sentiwiki.copernicus.eu/web/s3-olci-instrument) products are related to high performance of the sensor (from a radiometric and spectral point of view) for ocean color applications, ease of access to the datasets and a long-term commitment of the European Union to continue the series of Sentinel-3 missions under the Copernicus program. Standard Level 2 products were considered due to their high quality regarding the applied atmospheric correction procedures. Issues related to satellite data pre-processing and selection of the best atmospheric correction method are outside of the scope of this endeavor.

The Baseline Atmospheric Correction (BAC) with integrated Bright Pixel Correction (BPAC) is used by EUMETSAT for processing the standard Level-2 OLCI products. The algorithm is based on the initial procedure developed for MERIS (Antoine and Morel, 1999) and it was chosen in order to assure consistency between the two sensors. Since it was designed to perform well in open waters, a Bright Pixel Correction (BPAC) procedure was added to account for complex waters (Moore et al., 2017). The BPAC resolves situations where the NIR water-leaving radiance is no longer negligible, thus for high scattering waters (either high chlorophyll-a or SPM concentrations). The C2RCC (Case 2 Regional CoastColour) processor was originally developed for MERIS (Doerffer and Schiller, 2007) and was updated several times up to the current version, which is adapted to multiple satellite sensors, including OLCI. This neural network approach was designed to improve radiometric and biogeochemical parameters estimation in complex waters. While the C2RCC processor is also used when standard Level 2 datasets are derived, the resulting reflectance bands and atmospheric variables are not included in the distributed products, but only the following parameters are provided: Detrital and Dissolved Material absorption coefficient (ADG443), chlorophyll concentration (CHL_NN) and Total Suspended Matter concentration (TSM_NN). The latter one will be further used in this study.

The flags chosen to mask potentially contaminated pixels are the ones recommended by the report concerning Level 2 OLCI products (EUMETSAT, 2021). Extractions were performed using the average value over a 3x3 pixels window, centred on the in-situ sample location. Only those cases were considered when at least four valid measurements (out of nine values within one window) were available. Subsequent filtration was performed based on visual inspection of images, for cases where, although not flagged as bad pixels, the complexity and the heterogeneity of the sample location made the water-leaving reflectance values to be considered doubtable.

The remote sensing reflectance (R_{rs}) values provided by the MERM database were initially calculated by dividing the original in-situ fully normalized water-leaving reflectance by π. Therefore, in order to translate back from R_{rs} to ρ_w values, a simple multiplication with π was applied. Radiometric data aggregated within ±6 nm of OLCI sensor bands center wavelengths (490 nm, 560 nm, 665 nm and 865 nm), as provided by the authors, was used. More details concerning data acquisition, used protocols for post and pre-processing can be found in Zibordi et al. (2011) and Barker (2013a). No NIR wavelengths were available in case of MERM dataset.

2.4. Existing algorithms used for estimation of SPM and TUR

Several available algorithms for the estimation of SPM and TUR based on ρ_w were selected and their applicability for the western Black Sea basin was tested. The selection was performed taking into consideration those algorithms that were introduced by their authors as having global applicability. Certainly, many other regional approaches, for other areas of interest, are available, but these were not taken into consideration, since this is outside the scope of the current effort.

The first approach to be tested is the one delivered operationally by the standard OLCI Level 2 products, namely the TSM_NN. SPM values, denominated TSM in the output of the C2RCC neural network that deals with inherent optical properties (IOPs) and consequent biogeochemical variables, are computed using two of the five IOPs that the neural network is outputting. These are the b_{bp} – backscattering coefficient of suspended particulate matter, in m^{-1}, and b_{b_white} - backscattering by white particles, such as bubbles or coccolithophores, both computed at 442.5 nm wavelength (Brockmann et al., 2016). For simplicity reasons, the wavelength nomination will be discarded from further notations. These two IOPs add up to form the total backscattering (b_{b_total}), which is then used to estimate the SPM concentration. The parameters of the inversion equations can be adapted in order to account for regional differences of the particle assemblage composition and size characteristics. The current formulation used by C2RCC v2.1 (sometimes denoted also as NNv2) and implemented in the operational Collection 3

(EUMETSAT, 2021), is the following:

$$SPM = 1.06\ b_{b\_total}^{0.942} \quad (4)$$

while for previous products, under Collection 2 (before February 2021), the following approach was used (Doerffer, 2015):

$$SPM = 1.73\ b_{b\_total} \quad (5)$$

where b_{b_total} is the sum of b_{bp} and b_{b_white}.

Knowing these equations, used to predict SPM for both Collection 2 and Collection 3, it is possible to retrieve b_{b_total}. Then, using the relationship between this IOP and in-situ SPM measurements, we can derive regional adapted coefficients for eq. (4).

One of the first attempts to parameterize an algorithm to estimate turbidity and SPM that could be applied in multiple coastal areas, over a broad spectrum of water optical conditions, was the methodology proposed by Nechad et al. (2010). This semi-analytical algorithm will hereafter be denoted as NECHAD_SPM. It implies the usage of a single wavelength, providing that the selected band is chosen appropriately. The equation for this approach has the following form:

$$SPM = \frac{A\,\rho_w}{1 - \rho_{w\,/\,C}} \quad (6)$$

where A and C are two wavelength-dependent calibration coefficients and are provided in Nechad et al. (2010) at every 2.5 nm, for the spectral range between 520 nm and 885 nm. For $\rho_w(665)$ these are $A = 355.85$ and $C = 0.1725$, while for $\rho_w(865)$ $A = 2971.93$ and $C = 0.2115$ (Nechad et al., 2010; Van der Zande et al., 2022).

Han et al. (2016) reparametrized eq. (6) using a wider range of measurements, covering multiple regions around the Globe. Coefficients A and C are provided for both low and high SPM concentration ranges, as to be used in a multi-conditional algorithm with different wavelengths (red for low SPM and NIR for high SPM, with the boundary between the two classes empirically set at 100 g m^{-3}). The threshold to be used for transitioning from one to another is $\rho_w(665) < 0.09425$ and $\rho_w(665) > 0.12566$, respectively, with a combination between the two whenever $\rho_w(665)$ is between 0.09425 and 0.1256. To be noted that Han et al. (2016) used the R_{rs} in their study, instead of ρ_w, where $\rho_w(\lambda) = \pi R_{rs}(\lambda)$, and the original thresholds were $R_{rs}(665) < 0.03\ sr^{-1}$ and $R_{rs}(665) > 0.04\ sr^{-1}$. Our dataset does not show any $\rho_w(665) > 0.094$ (neither for DP or MERM), so the final tested coefficients where the ones proposed for low SPM conditions, meaning $A = 396.005$ and $C = 0.5$, using $\rho_w(665)$. Even if conditions are not met, the approach based on $\rho_w(754)$ will be also shown ($A = 2220.066$ and $C = 0.4029$). This algorithm will be further referenced as HAN.

Another tested methodology was the one described in Wei et al. (2021). The authors developed an algorithm with applicability over the global open ocean, coastal and inland waters. It makes use of $R_{rs}(\lambda)$ measurements at multiple wavelengths (blue, green, red and NIR) and predicts SPM based on two conditional formulations, for low and high concentrations. For the first category, a new parametrization is proposed, while for the second scenario the algorithm previously developed by Yu et al. (2019) is used. The original $R_{rs}(\lambda)$ data in their study were spectrally interpolated onto 410, 443, 486, 551, 671, 745 and 862 nm, in order to further apply the methodology to VIIRS (Visible Infrared Imaging Radiometer Suite) satellite data. As in HAN case, the samples were empirically split in two classes, based on the values of $R_{rs}(671)$: clear water when $R_{rs}(671) < 0.0008\ sr^{-1}$ (equivalent to $\rho_w(671) < 0.00251$) and turbid water if $R_{rs}(671) \geq 0.0012\ sr^{-1}$ (equivalent to $\rho_w(671) > 0.00377$) and a linear smoothing technique when $0.0008 \leq R_{rs}(671) < 0.0012$.

The formulation for the turbid waters (as in Yu et al., 2019) is the following:

$$SPM_{turbid} = B_1 \times I^{B_2} \quad (7)$$

where $B_1 = 20.43$ g m^{-3}, $B_2 = 2.15$ and I is a band-ratio term, which is modeled as:

$$I = C_0 \times \frac{R_{rs}(551)}{R_{rs}(486)} + \left[\frac{C_1 w_1 R_{rs}(671) + C_2 w_2 R_{rs}(745) + C_3 w_3 R_{rs}(862)}{R_{rs}(551)}\right] \quad (8)$$

where C_0, C_1, C_2, and C_3 are equal to 0.04, 1.17, 0.4, and 14.86, respectively; w represents a weighting factor, with:

$$w_i = \frac{R_{rs}(\lambda_i)}{R_{rs}(671) + R_{rs}(745) + R_{rs}(862)} \quad (9)$$

where the subscript i varies from 1 to 3, with λ_1, λ_2, and λ_3 corresponding to 671, 745, and 862 nm.

For clear waters, the following applies:

$$SPM_{clear} = \alpha_0 + \alpha_1 \times \left[\log_{10}\frac{R_{rs}(551)}{R_{rs}(443)}\right] + \alpha_2 \times \left[\log_{10}\frac{R_{rs}(551)}{R_{rs}(443)}\right]^2 \quad (10)$$

where $\alpha_0 = 0.5192$ m^{-3}, $\alpha_1 = 0.9278$ m^{-3}, and $\alpha_2 = 0.4291$ m^{-3}.

This algorithm will be further referenced as WEI.

For turbidity, the Nechad et al. (2009) approach is one of the algorithms to be tested (hereafter named NECHAD_TUR). The model has the same form as the one for SPM (eq. (6)), using a single band to retrieve TUR. The tested coefficients in this study are the recalibrated ones: $A = 610.94$ and $C = 0.2324$ for $\rho_w(665)$ and $A = 3030.32$, $C = 0.2115$ for $\rho_w(865)$. These versions are used for Copernicus Marine Service operational products (Van der Zande et al., 2022) and are close to the ones shown in Nechad et al. (2016). Following this work, Dogliotti et al. (2015) proposed the usage of a multi-conditional approach for scenarios characterized by large variability of TUR. This implies the combination of $\rho_w(645)$ for less turbid waters and $\rho_w(859)$ for more turbid scenarios. The switching thresholds were set at $\rho_w(645) < 0.05$ and $\rho_w(645) > 0.07$, with linear interpolation of TUR between these limits. This algorithm will be further referenced as DOGL and will be tested using $\rho_w(665)$ instead of $\rho_w(645)$ and $\rho_w(865)$ instead of $\rho_w(859)$, with A and C coefficients as in Van der Zande et al. (2022), which were already mentioned above.

Finally, a regionally calibrated model for TUR estimation based on $R_{rs}(645)$ was also considered (Constantin et al., 2016), hereafter denoted CONST. This was formulated using match-ups between in-situ TUR measurements (ranging between 2 and 160 NTU) and concurrent satellite (MODIS) derived $R_{rs}(645)$ values and used in several regional studies (Constantin et al., 2017; Cucu-Dumitrescu and Constantin, 2017). The equation has the following form:

$$TUR = 2.1663 \times e^{121.52\ R_{rs}(645)} \quad (11)$$

In order to test algorithms that entail the usage of spectral bands different from the ones available in our dataset (DP and MERM), which are Sentinel-3 OLCI specific, the multispectral shapes were interpolated to hyperspectral form, at 1 nm resolution. The Piecewise Cubic Hermitean Interpolation Polynomials method was used, since it is a shape-preserving approach, which does not alter the original input values. These high-resolution spectra were then used to compute sensor specific bands, using adequate spectral response functions, as needed: for VIIRS in case of WEI algorithm, or for MODIS when CONST was tested.

2.5. Multi-conditional algorithms blending thresholds

According to previous studies, SPM and TUR can be successfully predicted, using the green and red spectral bands, for low to moderate turbid waters (Nechad et al., 2010), up to approximately less than 60 g m^{-3}, according to Novoa et al. (2017). For higher concentration values, the use of NIR band(s) is recommended, since the water reflectance signal starts to saturate, first in the green, then in the red wavelengths, as TUR or SPM increases (Doxaran et al., 2002; Novoa et al., 2017; Luo et al., 2018).

Multi-conditional algorithms have been proposed as a solution to the difficulties in estimating SPM or TUR in complex water conditions over a wide range of particles composition, size and shape. For such situations, the use of only one spectral band can be associated to either low sensitivity or saturation issues (Dogliotti et al., 2015; Novoa et al., 2017; Han et al., 2016; Wei et al., 2021).

The difficulty in selecting the switching thresholds for different models, in the case of multi-conditional algorithms, has been previously acknowledged and documented (Novoa et al., 2017). These are usually chosen through trial and errors approaches. Novoa et al. (2017) opted for the determination of these thresholds after the comparison of spectral bands as follows: green against red and red versus NIR. After fitting a logarithmic regression curve, the intersection of the tangent line associated with the first derivative with the regression curve and the y axis was used as the value of saturation and, consequently, the value to be used for switching between algorithms (Table 3). For more details, please refer to the mentioned paper. As already described, Han et al. (2016) used $\rho_w(665)$ in order to transition from one model to another and the determined optimal values were set to 0.09425 and 0.1256, very similar to the ones proposed by Novoa et al. (2017) for the Gironde Estuary. Since in our dataset all $\rho_w(665)$ are below 0.09425, these thresholds are not applicable. Dogliotti et al. (2015) used $\rho_w(645)$ values of 0.05 and 0.07 to blend red and NIR estimations of turbidity, while Wei et al. (2021) approach uses the lowest values, compared to the other examples (Table 3).

3. Results and discussion

3.1. Relationships between SPM or TUR and water-leaving reflectance (ρ_w)

For our dataset, the covariance, in logarithmic scale, between both SPM and TUR with the ρ_w values tends to increase from short to long wavelengths. In case of SPM, when blue wavelengths are considered (in this case 490 nm), the scatter of data points is significant (Fig. 2a). The correlation between the two variables is better considering green (560 nm) and red (665 nm) wavelengths (Fig. 2b and c). Nevertheless, in these cases, and especially for the green part, important saturation effects can be noticed for medium SPM values (roughly above 8 g m^{-3}). This implies a poor potential estimation of SPM concentrations above this threshold when using such ρ_w products. This is not completely in line with other studies (Nechad et al., 2010; Novoa et al., 2017) that have shown that the use of the red band is suitable for estimation of SPM in low to medium turbid waters, thus for slightly higher values than those observed for our samples. However, when moving forward, towards the NIR spectral domain, it can be observed that a good, almost linear relation exists between the higher end of the SPM range and $\rho_w(865)$ (Fig. 2d; match-ups available only for the DP dataset). For low SPM values, it was noticed that NIR observations can be affected by the low intensity of the radiance recorded at sensor level and by the potential overestimation of the atmospheric effects (leading to over-corrections of the top-of-atmosphere reflectance values). Therefore, these wavelengths should not be used in such cases. The involvement of blue and green bands makes it prone to errors in areas where the atmospheric corrections process is problematic, such as coastal waters. All the above suggest the possibility to define a multi-conditional algorithm for SPM prediction using red (or even green) wavelengths in conjunction with the NIR ones.

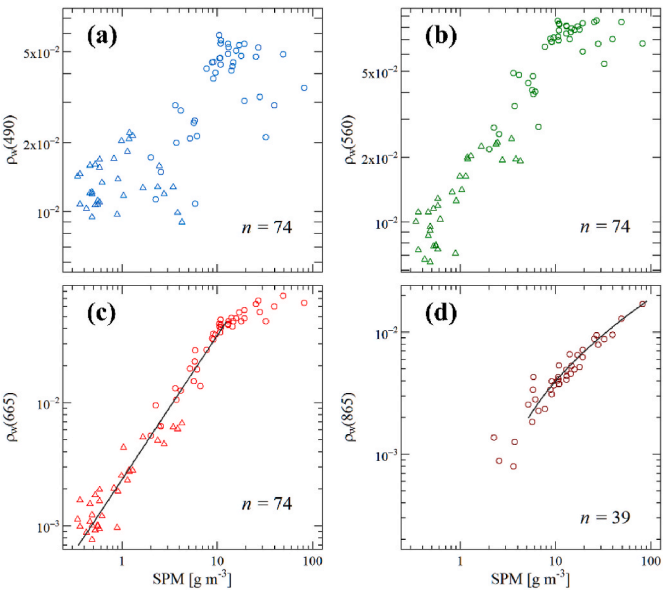

Fig. 2. The relationship between the concentration of Suspended Particulate Matter (SPM) and the water-leaving reflectance (ρ_w) at different wavelengths; triangles depict MERM samples, while circles show samples from the DP dataset; match-ups between SPM and $\rho_w(865)$ are available only for the DP dataset; solid black lines in c) and d) depict best fit regression models used in subsequent sections for algorithms development.

The same trends as for SPM can be observed for TUR: high degree of scatter for $\rho_w(490)$, saturation of $\rho_w(560)$ and $\rho_w(665)$ for medium to high TUR values and a relatively good covariance when $\rho_w(865)$ is considered (Fig. 3). The only minor difference is the relatively higher scatter between samples for low turbidity measurements and $\rho_w(560)$ or $\rho_w(665)$. Since these data points were available only for the DP locations, they characterize mostly medium to high turbidity conditions (Table 2) and conclusions cannot be drawn for all potential situations that can occur in the western part of the Black Sea basin. Thus, any derived algorithm using these samples will only be used to describe TUR conditions in very specific locations, such as the restricted area covered by the Danube River plume.

Table 3
Switching schemes for multi-conditional algorithms empowering two distinct wavelengths, from the red and NIR parts of the spectrum.

Study/Area	Parameter	Wavelength used as threshold (nm)	Lower limit (ρ_w)	Upper limit (ρ_w)
Novoa et al. (2017) (Gironde Estuary)	SPM	655	0.08	0.12
Novoa et al. (2017) (Bourgneuf Bay)	SPM	655	0.046	0.09
Han et al. (2016)	SPM	665	0.09425	0.1256
Wei et al. (2021)	SPM	671	0.00251	0.00377
Dogliotti et al. (2015)	TUR	645	0.05	0.07
Present study	SPM or TUR	665	0.018	0.045

3.2. Performance of existing algorithms for estimation of SPM and TUR

The first algorithm tested was the one that provides SPM estimates incorporated into the standard EUMETSAT marine Level 2 OLCI products (the TSM_NN), based on the C2RCC processor (Fig. 4a). As match-ups are available only from the DP samples, it was evaluated for SPM >2 g m^{-3} conditions. The transition from EUMETSAT Collection 2 to Collection 3, and from one model to estimate SPM to another, is clearly observed. New parameters used in Collection 3 improve the results, which is obvious in all associated statistics (e.g., *MdAPD* decreased from 226.9% to 58.03% and *RMSD* enhanced threefold). The main setback is the visible shift from the 1:1 line in both scenarios, shown by the high value of $MdR = 3.27$ (Collection 2) and $MdR = 1.58$ (Collection 3). The other associated statistics are satisfactory, with a slope for a model-II regression fit of 1.01 and 1.09, respectively, and $R = 0.93$ and 0.92.

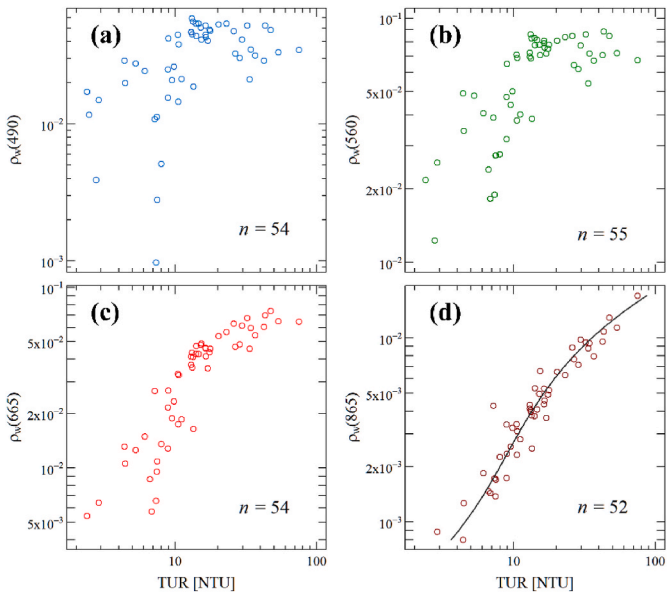

Fig. 3. The relationship between water turbidity (TUR) and the water-leaving reflectance (ρ_w) at different wavelengths; match-ups available only for the DP dataset; solid black line in d) depict best fit regression model used in subsequent sections for algorithm development.

This suggests that a regional recalibration of the model could be proposed, with adapted coefficients.

NECH_SPM single band algorithm was tested for both $\rho_w(665)$ and $\rho_w(865)$ (Fig. 4b and c). The red band shows good predictions for low SPM, but overestimates in the region of medium values, above approximately 8 g m^{-3}. For higher concentrations, the saturation effects become visible and affect the performance of the model. For the NIR band, however, the predictions are significantly improved for medium to high SPM concentrations, with a MdAPD of only 15.66%. Based on these observations, it is reasonable to expect a good performance of a multi-conditional algorithm that combines both spectral regions, with locally adjusted coefficients for the models.

When considering the parameters proposed by Han et al. (2016), the underestimation for low SPM values and the overestimation of medium SPM concentrations by the $\rho_w(665)$ model slightly decrease (Fig. 4d). As expected, the saturation effects continue to influence the higher end of the samples (above 20 g m^{-3}). While it represents an incremental improvement over the NECH_SPM parameterization, it still lacks the capacity to correctly account for high SPM values.

This is simply because the model designed for these conditions, based on $\rho_w(754)$, is not used for SPM estimation, since there is no situation with $\rho_w(665) > 0.094$ (the threshold above which the authors suggest to rely on $\rho_w(754)$ instead of $\rho_w(665)$). Nevertheless, the $\rho_w(754)$ model was also tested (Fig. 4e). Similar to NECH_SPM_865, it shows better predictions for the higher SPM range, compared to the red band approach, but still requires a finer tuning of coefficients.

The final algorithm, for which performances were assessed, was WEI (Fig. 4f). For higher concentrations, the predictions are satisfactory, although a general tendency to underestimate SPM is visible. The parameterization for clear waters, however, is proved not to be suitable for our region of interest. Tailored coefficients for eq. (10) might improve the results, but it could not provide expected results in scenarios where, even for clear waters, the SPM does not covary with the chlorophyll-a concentration, which drives the changes in the blue to green ratio. Last, but not least, WEI is expensive in terms of required spectral values, using no less than six wavebands, over the entire RGB-NIR domain. A contamination or processing error in any band could potentially degrade the final SPM estimation.

For TUR, the NECH_TUR approaches (Fig. 5a and b), using $\rho_w(665)$ and $\rho_w(865)$, show similar patterns as the ones observed for SPM scenarios, with an overall higher degree of scatter in data points. Again, the NIR approach performs reasonably well, with the potential to be even

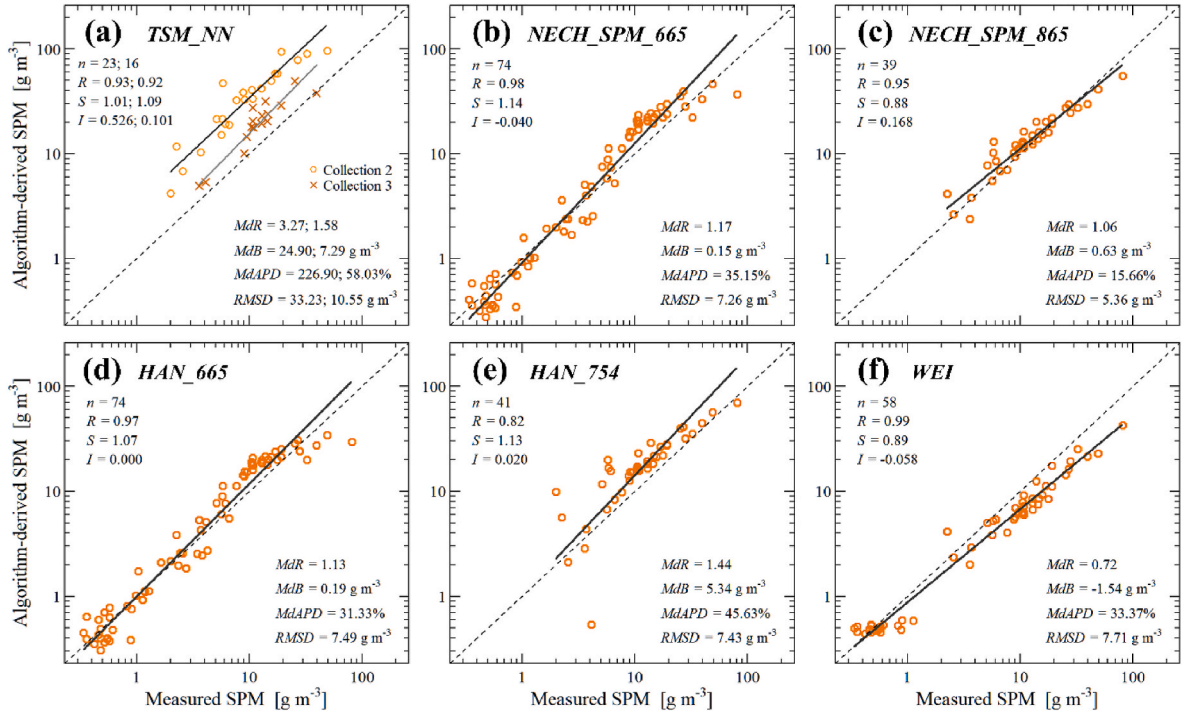

Fig. 4. Scatterplots between in-situ measured SPM and algorithm-derived SPM, based on several models; black solid lines depict model-II linear regression fit; shown statistical parameters are based on not log-transformed values, except correlation coefficient *R*, slope *S* and intercept *I*; for a) two sets of statistical parameters are shown, one for samples derived from products under EUMETSAT's Collection 2 and another one, after the semicolon, computed based on Collection 3; two distinct model-II linear regression fits are also provided, for each collection.

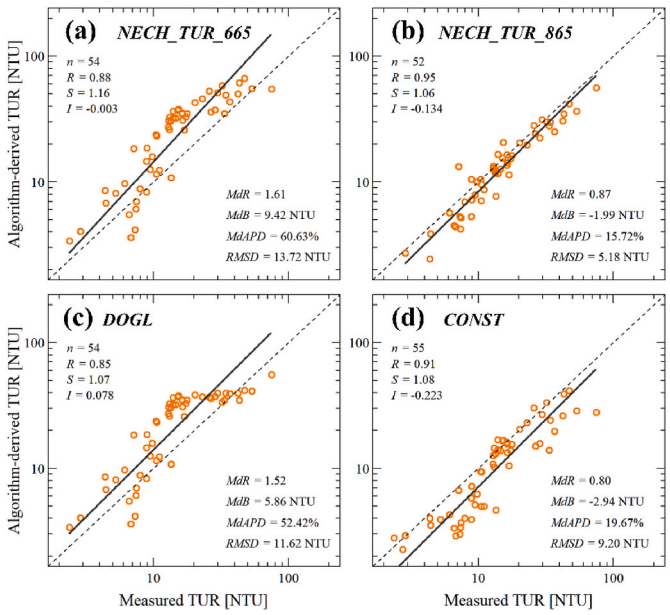

Fig. 5. Scatterplots between in-situ measured TUR and algorithm-derived TUR, based on several models; black solid lines depict model-II linear regression fit; shown statistical parameters are based on not log-transformed values, except correlation coefficient *R,* slope *S* and intercept *I*.

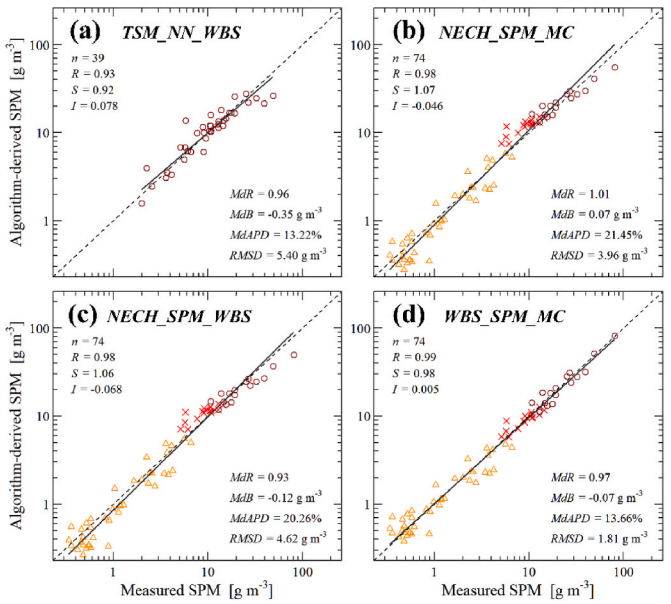

Fig. 6. Scatterplots between in-situ measured SPM and algorithm-derived SPM, based on several regional adapted models; black solid lines depict model-II linear regression fit; shown statistical parameters are based on not log-transformed values, except correlation coefficient *R,* slope *S* and intercept *I*; for b), c) and d) data points depicted as orange triangles, dark red open circles and red cross-marks represent the SPM values estimated using $\rho_w(665)$, $\rho_w(865)$ and merged scheme between these two, respectively. (For interpretation of the references to colour in this figure legend, the reader is referred to the Web version of this article.)

more improved if model coefficients are regionally adapted. As expected, the DOGL example (Fig. 5c), being a combination of the two previous ones, shows comparable results. All values below 20 NTU are estimated using $\rho_w(665)$ and exhibit high scatter. For the others, one is predicted using the NIR band, while the rest are the blended version between the algorithms. It suggests that the switching scheme thresholds (Table 3) might be too high for this region of interest and that changing these boundaries can be the key to a better performance algorithm.

Finally, the only regionally developed algorithm for TUR retrieval based on optical data, CONST, was also evaluated (Fig. 5d). It performs well in terms of *MdAPD* (19.67%) and *S* (1.08), but shows a tendency to underestimate TUR, which is highlighted by statistics such as *MdR* (0.8), *MdB* (−2.94 NTU) and *RMSD* (9.20 NTU). These shortcomings can have multiple origins, given the fact that the algorithm was initially developed based on in-situ TUR match-ups with MODIS derived $\rho_w(645)$. Differences in satellite data processing (especially atmospheric corrections), in spectral and radiometric characteristics of MODIS and OLCI bands are just the most significant factors that can influence the accuracy of the algorithm when translated and applied to Sentinel-3 data.

3.3. Regional parameterization of SPM and TUR algorithms

3.3.1. Regional adaptation of TSM_NN coefficients

One easy approach to obtain SPM concentration products when using Sentinel-3 OLCI data is to rely on the outputs of the C2RCC neural network. Since, as previously shown, the default coefficients that are used to translate IOPs (b_{b_total}) to SPM are not adapted to our region of interest, a re-calibration was performed based on the match-ups with in-situ data. Consequently, eq. (4) becomes:

$$SPM = 0.712\, {b_{b\_total}}^{0.898},\ \text{with } n = 39 \tag{12}$$

Using this new formulation (TSM_NN_WBS), the estimation of SPM values gains in overall accuracy (Fig. 6a), with $MdAPD = 13.22\%$ and $MdB = -0.35$ g m^{-3} as best statistical parameters examples in this regard. Even more, the less favourable statistics are determined by several high SPM values. The algorithm predicts very well for SPM <20 g m^{-3}. If only these samples were used, then $MdB = -0.13$ g m^{-3}, $MdAPD = 12.03\%$ and $RMSD = 2.46$ g m^{-3}. However, the adaptation of the coefficients to the regional specificities was performed using only samples from the Danube River plume area, with SPM concentrations above 2 g m^{-3}. For clear waters, the proposed solution needs to be further tested and adapted, if necessary. There are two options for using the regional coefficients proposed here. One refers to situations when standard Level 2 Sentinel-3 OLCI products are used as inputs. In this case, knowing the methodology applied to derive SPM (see eq. (4) or (5)), it is possible to derive b_{b_total}, which can be further inserted in eq. (12). The second scenario refers to in-house processing of Level 1 Sentinel-3 OLCI products using the C2RCC neural network. For this approach, the regional coefficients can be manually specified, with *TSM factor* = 0.712 and *TSM exponent* = 0.898. The SNAP C2RCC processor still has some limitations in terms of maximum SPM values that can be derived. The scaling factor was modified in the last NN version (EUMETSAT, 2021) as to allow a maximum output of 400 g m^{-3}, compared to 100 g m^{-3} in the previous variant. Still, some exceptionally rare high discharge events might not be properly accounted for, but such scenarios can only impact very small areas right in front of the river mouths. The same limitation is valid for the other approaches as well, since the calibration data used in this study do not cover very high turbid scenarios.

3.3.2. Regional adaptation of blending thresholds for multi-conditional algorithms implementation

One of the main conclusions from the previous sections refers to the necessity of developing multi-conditional algorithms that use more than one spectral band to account for wide variations in the SPM concentration range. To this regard, one of the main challenges is to establish a suitable switching approach. In order to determine the optimal threshold(s) for the transition between red and NIR based algorithms, the relations between $\rho_w(665)$ and SPM or TUR (Fig. 2c and 3c) were analyzed. These show a linear correlation for low to medium concentrations, with increased scatter towards the higher end, due to saturation

effects. For all potential cases where $\rho_w(665)$ increases gradually from 0.001 to 0.06, with an increment of 0.0005 (thus totaling 119 scenarios), the correlation coefficient (R) was computed between the two variables, using the normal values (not log-transformed), since these ones better highlight the saturation conditions. R progressively increases up to approximately 0.98, after which tends to decrease, as the red band starts to become less useful in predicting SPM concentration on a linear relation. This turning point corresponds to $\rho_w(665) = 0.045$, which can be identified as a flexing spot using a visual interpretation of Fig. 2c–as well. Therefore, it is considered that $\rho_w(665) = 0.045$, which corresponds to roughly 12 g m^{-3} (based on a linear fit model, shown as a solid line in Fig. 2c), to be the upper limit for which $\rho_w(665)$ should be used to estimate SPM in the western basin of the Black Sea. For the transition zone, since $\rho_w(865)$ can account for concentrations as low as 5 g m^{-3} (Fig. 2d), it is proposed that the merging scheme to be applied whenever $0.018 \leq \rho_w(665) \leq 0.045$ (Table 3). The lower value (0.018) was set based on the same test that uses R computed between $\rho_w(865)$ and SPM and corresponds to a value of approximately 5 g m^{-3}.

3.3.3. Regional calibration of the Nechad SPM approach

Considering the above, it was evaluated how a combined NECH_SPM approach, using both $\rho_w(665)$ and $\rho_w(865)$ (as in Fig. 4b plus 4c) into a single multi-conditional algorithm (hereafter denoted NECH_SPM_MC) will better account for various SPM concentrations when compared to the usage of a single band. Indeed, using such an alternative, the algorithm-derived SPM concentrations are significantly better, over the entire range, compared to only using a single band (Fig. 6b). To be noted that the tailored switching thresholds, described in the previous chapter, were used. If coefficients A and C from eq. (6) are regionally calibrated ($A = 358.228$, $C = 0.5$ for $\rho_w(665)$ and $A = 2366.356$, $C = 0.05$ for $\rho_w(865)$), using a non-linear regression analysis, in logarithmic space, the quality of the results does not significantly change (e.g. $S = 1.04$, $MdR = 0.95$, $MdB = -0.1$ g m^{-3}, $MdAPD = 18.25\%$, $RMSD = 3.32$ g m^{-3}). But, since parameter C, which represents the ratio between specific particulate back-scattering and absorption coefficients, was originally calibrated using standard IOP data (Nechad et al., 2010), a more suitable alternative is to use the values for C as tabulated by the original study and only regionally adapt for A. Apart from the reasons exposed before, it should also be mentioned that C has negligible impact in the linear regime, where the algorithm is mainly used. Following this schema, we get $A = 338.634$ for $\rho_w(665)$ and $A = 2672.883$ for $\rho_w(865)$ (Table 4). The outcomes, in this case (NECH_SPM_WBS), are similar to the default NECH_SPM_MC and to the version when also C was regionally calibrated (see above). In fact, all three approaches are characterized by comparable statistics, due to the similar values for the A parameter (Tables 4 and 5). Thus, eq. (6), with regional adaption for A, becomes:

$$SPM_{red} = \frac{338.634\,\rho_w(665)}{1 - \rho_w(665)/0.1725} \quad (13)$$

for $\rho_w(665)$, respectively clear waters ($n = 58$), and

$$SPM_{NIR} = \frac{2672.883\,\rho_w(865)}{1 - \rho_w(865)/0.2115} \quad (14)$$

for $\rho_w(865)$, respectively turbid waters (n = 33). A bootstrap run on the dataset resulted in median values of $\log_{10}(A) = 2.529$ (with $\sigma = 0.069$) for $\rho_w(665)$ and $\log_{10}(A) = 3.426$ (with $\sigma = 0.047$) for $\rho_w(865)$. Logarithmic values are provided since, are mentioned, the regression is performed in logarithmic space. These translate to $A = 338.468$ for $\rho_w(665)$ and $A = 2667.163$ for $\rho_w(865)$, which are very close to the above mentioned ones (in eqs. (13) and (14)), which were computed using the initial data. Overall, it could be assumed that the regression analysis performed on the original values did not overfit the model.

The merging between the two is performed when $0.018 \leq \rho_w(665) \leq 0.045$, using a linear smoothing function:

$$SPM = (1 - w) \times SPM_{red} + w \times SPM_{NIR} \quad (15)$$

where SPM_{red} is the SPM calculated using the red band and SPM_{NIR} is the one computed based on the NIR band; w is the weight of the algorithm, changing linearly from 0 at $\rho_w(665) = 0.018$ to 1 at $\rho_w(665) = 0.045$, thus $w = 37.03704 \times [\rho_w(665) - 0.018]$.

3.3.4. Regional algorithms using the red and NIR wavelengths for SPM estimation

Apart from the re-calibration of existing algorithms, a new, tailored empirical method can also be derived. Based on the relation between ρ_w and SPM, several approaches, in terms of used bands and their combination, were tested. The best statistical outputs were obtained when a linear model for $\rho_w(665)$ (black solid line in Fig. 2c) and a second order polynomial algorithm for $\rho_w(865)$ (black solid line in Fig. 2d) are combined (Fig. 6d). The corresponding formulae are:

$$SPM_{red} = 10^{[2.24239 + 0.85601\ R_r]} \quad (16)$$

where SPM_{red} is the predicted SPM concentration for clear waters ($n = 58$), based on a red spectral band (in this case $\rho_w(665)$) and $R_r = \log_{10}[\rho_w(665)]$.

$$SPM_{NIR} = 10^{[6.75172 + 3.68182\ R_N + 0.53541\ (R_N)^2]} \quad (17)$$

where SPM_{NIR} is the predicted SPM concentration for turbid waters ($n = 33$), based on a NIR spectral band (in this case $\rho_w(865)$) and $R_N = \log_{10}[\rho_w(865)]$. The merging between SPM_{red} and SPM_{NIR} is done using eq. (15). The bootstrap analysis showed median coefficients of 2.24275 ($\sigma = 0.043$) and 0.85623 ($\sigma = 0.021$) for eqs. (16) and (6.71243) ($\sigma = 1.672$), 3.64927 ($\sigma = 1.517$) and 0.52956 ($\sigma = 0.342$) for eq. (17). Again, the median values of coefficients are similar, almost identical for the linear model based on $\rho_w(665)$, with the ones obtained based on the original dataset. Standard deviation for the NIR parameterization is higher and might signal some overfitting.

This last algorithm (WBS_SPM_MC) yields the best estimates for SPM, for the western Black Sea basin and has the potential to cover a significant range of concentrations. The associated statistics show a $MdAPD$ as low as 13.66%, a MdR close to 1 (0.97), low $RSMD$ (1.81 g m^{-3}) and MdB (−0.07 g m^{-3}).

3.3.5. Regional calibration of the Nechad TUR approach

For turbidity, combining $\rho_w(665)$ and $\rho_w(865)$ into one multi conditional algorithm (NECH_TUR_MC), with default coefficients (but with regionally adapted thresholds for the switching between models), resulted in a satisfactory estimation of turbidity (Fig. 7a), with $MdAPD$

Table 4
Default coefficients (parameters for eq. (6)) for the Nechad approach to estimate SPM and TUR (Nechad et al., 2010; Van der Zande et al., 2022) and the regionally proposed coefficients for the western Black Sea basin.

	SPM				TUR			
	665 nm		865 nm		665 nm		865 nm	
Parameter	A	C	A	C	A	C	A	C
Nechad default	355.85	0.1725	2971.93	0.2115	610.94	0.2324	3030.32	0.2115
Nechad regional	338.634	0.1725	2672.88	0.2115	413.314	0.2324	3537.12	0.2115

Table 5
Performance of existing and newly calibrated models for estimation of SPM and TUR using ρ_w; inputs marked with * show SPM algorithms that were tested or calibrated based only on the DP samples.

Algorithm/Associated statistics	*n*	*R*	*S*	*I*	*MdR*	***MdB*** **(g m^{-3} or NTU)**	*MdAPD* (%)	***RMSD*** **(g m^{-3} or NTU)**
SPM - existing algorithms								
TSM_NN Collection 2*	23	0.93	1.01	0.526	3.27	24.9	226.9	33.23
TSM_NN Collection 3*	16	0.92	1.09	0.101	1.58	7.29	58.03	10.55
NECH_SPM_665	74	0.98	1.14	−0.040	1.17	0.15	35.15	7.26
NECH_SPM_865*	39	0.95	0.88	0.168	1.06	0.63	15.66	5.36
HAN_665	74	0.97	1.07	0.000	1.13	0.19	31.33	7.49
HAN_754*	41	0.82	1.13	0.020	1.44	5.34	45.63	7.43
WEI	58	0.99	0.89	−0.058	0.72	−1.54	33.37	7.71
SPM - regionally calibrated algorithms								
TSM_NN_WBS*	39	0.93	0.92	0.078	0.96	−0.35	13.22	5.40
NECH_SPM_MC	74	0.98	1.07	−0.046	1.01	0.07	21.45	3.96
NECH_SPM_WBS	74	0.98	1.06	−0.068	0.93	−0.12	20.26	4.62
WBS_SPM_MC	74	0.99	0.98	0.005	0.97	−0.07	13.66	1.81
TUR - existing algorithms								
NECH_TUR_665	54	0.88	1.16	−0.003	1.61	9.42	60.63	13.72
NECH_TUR_865	52	0.95	1.06	−0.134	0.87	−1.99	15.72	5.18
DOGL	54	0.85	1.07	0.078	1.52	5.86	52.42	11.62
CONST	55	0.91	1.08	−0.223	0.8	−2.94	19.67	9.20
TUR - regionally calibrated algorithms								
NECH_TUR_MC	54	0.91	0.83	0.210	1.01	0.13	18.12	5.38
NECH_TUR_WBS	54	0.93	1.14	−0.177	1.04	0.49	16.81	3.88
NECH_TUR_NIR	52	0.95	1.05	−0.058	1.02	0.16	14.66	3.85
WBS_TUR_NIR	52	0.96	0.96	0.046	0.97	−0.21	10.51	3.83

= 18.12% and *RMSD* = 5.38. If coefficient *A* is regionally re-calibrated (Table 4) using the in-situ measurements (NECH_TUR_WBS, Fig. 7b), we get:

$$\mathrm{TUR}_{\mathrm{red}} = \frac{413.314\,\rho_w(665)}{1 - \rho_w(665)/0.2324} \tag{18}$$

for $\rho_w(665)$, with $n = 33$, and

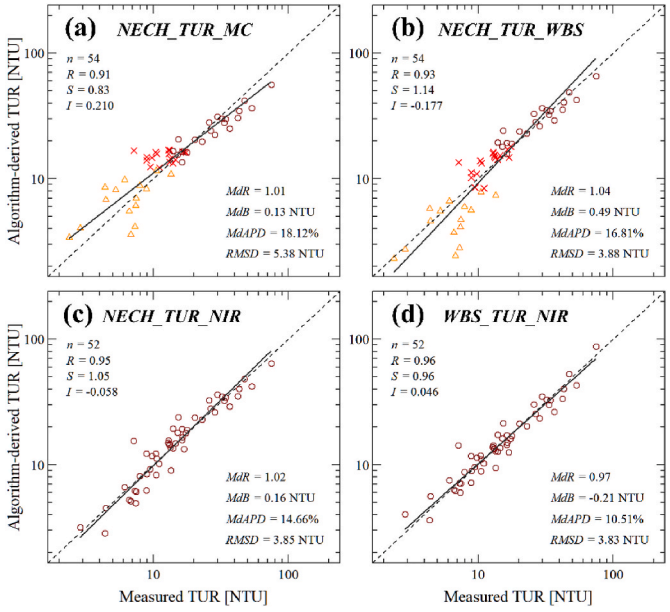

Fig. 7. Scatterplots between in-situ measured TUR and algorithm-derived TUR, based on several regional adapted models; black solid lines depict model-II linear regression fit; shown statistical parameters are based on not log-transformed values, except correlation coefficient *R*, slope *S* and intercept *I*; for a) and b) data points depicted as orange triangles, dark red open circles and red cross-marks represent the TUR values estimated using $\rho_w(665)$, $\rho_w(865)$ and merged scheme between these two, respectively. (For interpretation of the references to colour in this figure legend, the reader is referred to the Web version of this article.)

$$\mathrm{TUR}_{\mathrm{NIR}} = \frac{3537.122\,\rho_w(865)}{1 - \rho_w(865)/0.2115} \tag{19}$$

for $\rho_w(865)$, with $n = 52$.

Unlike the case of SPM, all samples were used to calibrate the NIR-based model, not only those for which $\rho_w(665) > 0.018$. This decision was taken considering the good correlation between $\rho_w(865)$ and TUR extending towards the lowest turbidity values (Fig. 3d). The merging between the two is done using eq. (15), with TUR instead of SPM, whenever $0.018 \le \rho_w(665) \le 0.045$.

A bootstrap run on the dataset resulted in median values of $\log_{10}(A) = 2.617$ ($\sigma = 0.036$) for $\rho_w(665)$ and $\log_{10}(A) = 3.548$ ($\sigma = 0.037$) for $\rho_w(865)$. Thus, $A = 413.929$ for $\rho_w(665)$ and $A = 3536.930$ for $\rho_w(865)$, which are very close to the above mentioned ones (in eqs. (18) and (19)), computed using the original data.

Compared to the scenario based on the default parameter *A*, this approach yields marginally better outcomes (Fig. 7b). This only slight increase of accuracy is partly caused by persisting high scattering of samples covering the low range of the relation between TUR and $\rho_w(665)$ (Fig. 3c). An alternative approach would be to rely on a single spectral band, $\rho_w(865)$, to predict TUR for the entire range (all TUR algorithms proposed here have applicability over 2 NTU). Using only the NIR model (NECH_TUR_NIR – eq. (19) and Fig. 7c), the estimations are enhanced, especially in term of slope of the linear fit (*S*) and *MdAPD* (Table 5).

3.3.6. Regional algorithm using the NIR wavelengths for TUR estimation

Finally, a regional, empirical algorithm for TUR prediction using the NIR information was defined (WBS_TUR_NIR – Fig. 7d). It is based on a third order polynomial fit between the log-transformed values of $\rho_w(865)$ and TUR (black solid line in Fig. 3d). As expected, since this was calibrated using all available in-situ local data, it provides the best estimates, compared to the others. The equation is the following:

$$\mathrm{TUR}_{\mathrm{NIR}} = 10^{\left[13.19129 + 12.49285\,R_N + 4.46672\,(R_N)^2 + 0.56504\,(R_N)^3\right]} \tag{20}$$

where $\mathrm{TUR}_{\mathrm{NIR}}$ is the predicted TUR concentration, based on a NIR wavelength (in this case $\rho_w(865)$) and $R_N = \log_{10}[\rho_w(865)]$, with $n = 52$. The bootstrap analysis results (medians) are 13.69246 ($\sigma = 5.951$), 13.15807 ($\sigma = 7.481$), 4.774393 ($\sigma = 3.111$) and 0.60241 ($\sigma = 0.428$)

for coefficients in eq. (20). Compared to the other regional algorithms shown in previous sections, the differences are slightly higher in this case, suggesting a potential overfitting of the algorithm on the original data. The distribution of match-ups, used to derive this equation, is not the same for all ranges of TUR (Fig. 3d). There are only few measurements for the low and high end, which can potentially trigger such differences. While not necessarily incorrect, it is not possible to decide if there is an overfitting or not. This issue remains to be resolved if supplementary data will become available.

The usage of the NIR spectral information to infer values of SPM (and TUR) for medium to relatively low concentrations might appear arguable, given the fact that this part of the electromagnetic spectrum has been predominantly used for moderate to high SPM and TUR ranges. However, we have shown that NIR data, both in-situ or from satellite, correlate well with the two biogeochemical variables. Additionally, within this study, we do not recommend the usage of NIR bands for the estimation of low SPM (<5 g m^{-3}) or very low TUR (<2 NTU). In fact, most of the validation activities conducted to assess the quality of the Sentinel-3 OLCI NIR bands were based on fiducial reference measurements collected by sensors located in generally clear waters. In particular for the Black Sea, the AERONET_OC stations (the main source of data for in-situ radiometric measurements for validation purposes), are located in the western Black Sea (Gloria and Galata). These areas are less influenced by riverine inputs (thus characterized by relatively clear waters). Consequently, most of the in-situ $\rho_w(865)$ observations used to validate algorithms in the region (EUMETSAT's report on Collection 3, 2021) recorded values below 0.002, while our proposed algorithms generally make use of $\rho_w(865)$ above this threshold (Fig. 2d and 3d). In other words, it becomes difficult to assess the accuracy of the NIR bands in medium turbid waters in the absence of adequate in-situ radiometric data. Nevertheless, the observed good correlation between $\rho_w(865)$ and SPM or TUR is an indirect indication that the NIR bands have the potential to be used for such purposes, given that the ranges of applicability are respected.

Applying the proposed regional algorithms to Sentinel-3 OLCI images reveals consistent SPM and TUR products, with coverage of a wide range of values and with seamless transition from low to high concentrations. In Fig. 8, two distinct cases are shown. First, an image from May 31st, 2020, covering the entire western Black Sea (Fig. 8a, b and c) unravels the intricate patterns of the SPM concentration. In this particular example, marginal areas, generally overlapping the continental shelf, are characterized by values of 2–3 g m^{-3}. Concentrations increase in the vicinity of the Danube plume, to approximately 5 g m^{-3} and up to 20–25 g m^{-3} in isolated parts in front of river mouths. Central regions are characterized by low SPM, below 1 g m^{-3}. Fig. 8a and b shows the SPM maps generated using the two proposed algorithms, WBS_SPM_MC and NECH_SPM_WBS. On a visual inspection, both seem to have identical, or at least similar, values. However, differences exist (Fig. 8c): green to blue areas (which generally overlap medium SPM concentrations regions) show pixels where NECH_SPM_WBS overestimates the SPM values when compared to WBS_SPM_MC (with more than 20%). Red hues pixels indicate the opposite situation, with values of −30% in the deep-sea parts. Note that, given the low values of SPM here, 30% deviations account for absolute differences of less than 0.2 g m^{-3}.

The second example concentrates on a smaller geographical area, in front of Danube mouths (Fig. 8d, e and f), with a high range of concentration, from less than 1 g m^{-3} to almost 100 g m^{-3}. The image was captured on April 13th, 2018. The differences between the two SPM algorithms can be as high as 30 or 40 g m^{-3} in areas of high concentrations (with approximately 90–100 g m^{-3} according to WBS_SPM_MC), very close to the river mouths. Medium concentrations regions (6–10 g m^{-3}) are characterized by differences ranging from 1 to 2 g m^{-3} (around 20%), while clear waters are again represented by an underestimation of NECH_SPM_WBS of roughly 30%. For the same image, TUR maps are also shown (Fig. 8g, h and i), based on WBS_TUR_NIR and NECH_TUR_NIR algorithms. Given the range of applicability of the method, maps show only pixels with values >2 NTU. It can be observed that the usage of the NIR spectral band provides satisfactory outputs. Some salt and pepper noise is visible for low ranges, given the low ρ_w values. Moderate to high turbidity areas are less affected. River plumes shapes and patterns can be clearly observed. The differences between the two maps have the same spatial patterns as for SPM, with slightly higher underestimation by NECH_TUR_NIR in clear waters.

4. Conclusions

This study focused on regional challenges linked to the estimation of SPM and TUR using ρ_w, in the western Black Sea. This marine basin is sensitive to changes dictated by natural events and human activities, especially due to its reduced size and limited connection with the global ocean. It is essential, for a proper management, to have accurate and timely information regarding the dynamics of various biogeochemical variables. Therefore, robust retrievals of SPM and TUR using satellite information is important for filling the knowledge gaps and provide quality data for further research and policy implementation. While its operational applicability is limited to the western Black Sea basin, the theoretical concepts approached in this study can be applied in any other region to ensure better performance of the algorithms used to derive biogeochemical variables from radiometric measurements. It was shown that, although some of the existing algorithms can provide good estimates, fine tuning using local data can improve the overall accuracy (please refer to statistics shown in Table 5). Also, the usage of a multi-conditional approach is mandatory in most of the situations, since the Black Sea offers a wide range of conditions from optical active constituent's point of view. One of the main setbacks is represented by the lack of independent in-situ data for the validation of satellite products. We had to tackle a situation when in-situ measurements for both model calibration and validation are scarce and might require blending of different data sources for algorithm development. However, using the limited available information, regional calibration was performed, which represents a first step towards robust processing chains for Earth Observation information. Also, the good correlation between SPM or TUR and ρ_w values can be considered, in its own, an indirect validation and an argument for the quality provided by the Sentinel-3 OLCI standard Level 2 products. Given the in-situ data used for the calibration of these regional algorithms, turbidity estimations should be considered accurate only in cases with medium to high NTU values. Applicability of the SPM algorithm extends further, towards clearer waters. Nevertheless, results in low SPM concentration areas should be treated with care when applied to satellite data, since the calibration was performed, for this low range, based on few samples which do not represent direct match-ups with Sentinel-3 derived ρ_w. Another important conclusion is that NIR wavelengths can be successfully used to retrieve both SPM and TUR, even for moderate to low turbidity conditions. New thresholds to be used for the switching scheme of a multi-conditional algorithm have been defined, as well. These are significantly different from other similar approaches (Table 3) and can increase the quality of the final products.

The algorithms proposed by this study do not fully apply for exceptional events, when very high SPM and TUR values can be registered at the Danube River mouths, up to several hundreds of g m^{-3} or NTU. Such circumstances, triggered mainly by high intensity precipitation episodes which lead to flash floods in the Danube hydrological basin, are becoming more frequent (Constantin, 2022). However, these are very limited events, both in terms of spatial and temporal extension. While the parameterized NIR algorithms have the potential to portray even such scenarios, the exact accuracy of the predicted SPM and TUR values cannot be assessed beyond the training domain. For such situations, additional data will be required to further expand the algorithm's operation range.

When applied to satellite images, even algorithms that seem to have similar accuracies can yield maps of SPM or TUR with important

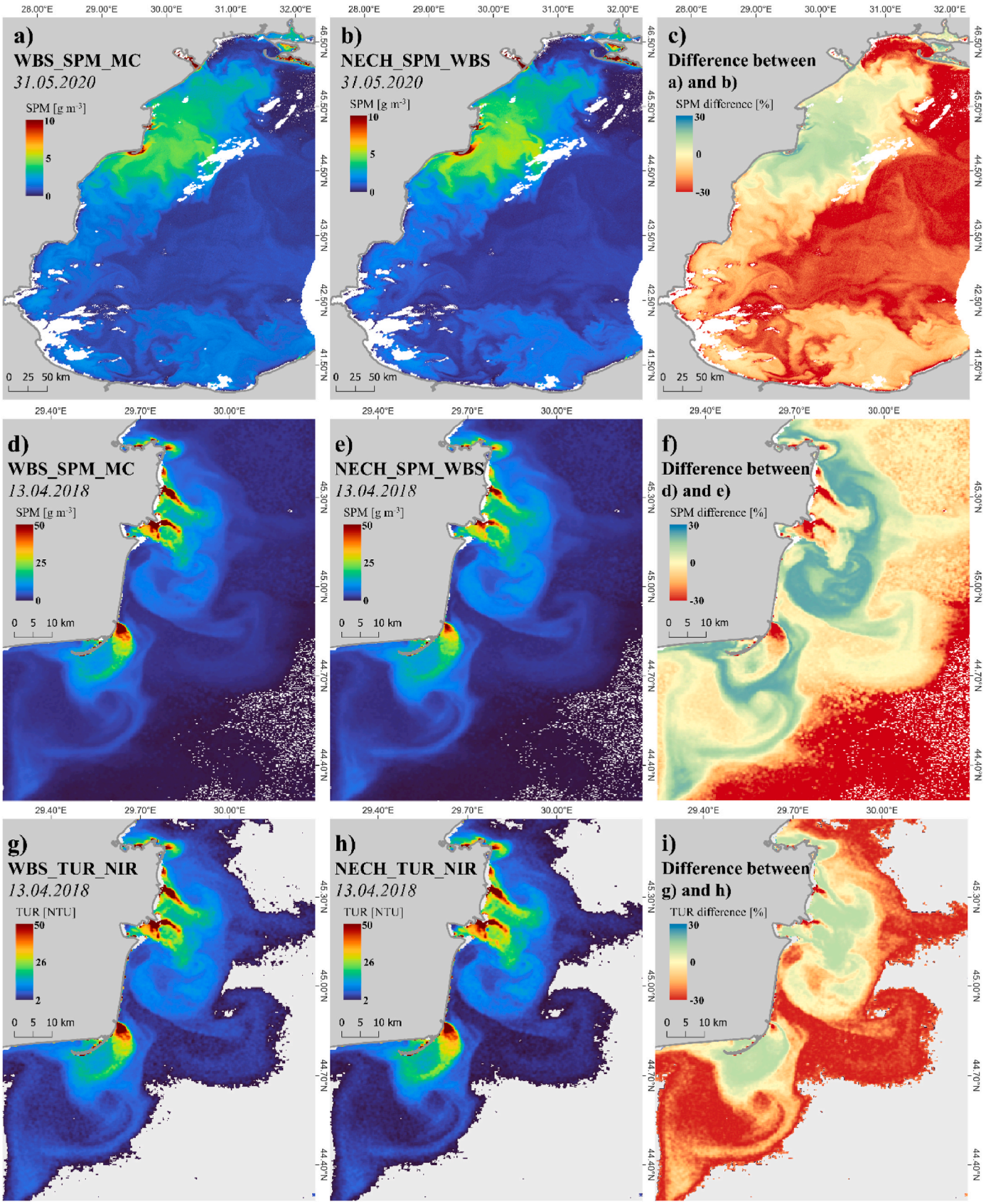

Fig. 8. a) and d) SPM derived from the WBS_SPM_MC algorithm; b) and e) SPM derived from the NECH_SPM_WBS; c) and f) relative differences in percentages between WBS_SPM_MC and NECH_SPM_WBS estimated SPM concentrations; g) TUR derived from the WBS_TUR_NIR algorithm; h) TUR derived from the NECH_TUR_NIR; and i) relative differences in percentages between WBS_TUR_NIR and NECH_TUR_NIR estimated water turbidity values.

differences in specific areas. Therefore, it is important to know the characteristics of each applied methodology and correctly select the one (s) that better suit the application's needs. Overall, the SPM concentration and TUR can be accurately derived for the western Black Sea basin, using water-leaving reflectance data in the red and NIR spectral domain, either measured in-situ or acquired by satellites. Next endeavors could focus on validation of these algorithms when applied to satellite images, based on independent in-situ measurement. Testing the applicability on other satellite sensors, such as the higher spatial resolution Sentinel-2 MSI (MultiSpectral Instrument), would also contribute to further closing the existing knowledge gaps.

CRediT authorship contribution statement

Sorin Constantin: Writing – review & editing, Writing – original draft, Methodology, Formal analysis, Data curation, Conceptualization, Visualization. **Ioan-Daniel Șerban:** Writing – review & editing, Validation, Visualization. **David Doxaran:** Writing – review & editing. **Fabrizio D'Ortenzio:** Writing – review & editing.

Declaration of competing interest

The authors declare the following financial interests/personal relationships which may be considered as potential competing interests:

Sorin Constantin reports financial support was provided by Romanian Ministry of Education and Research, CNCS - UEFISCDI. Sorin Constantin reports financial support was provided by European Space Agency. Ioan-Daniel Serban reports financial support was provided by European Space Agency. David Doxaran reports financial support was provided by European Space Agency. Fabrizio D'Ortenzio reports financial support was provided by European Space Agency. If there are other authors, they declare that they have no known competing financial interests or personal relationships that could have appeared to influence the work reported in this paper.

Data availability

Data will be made available on request.

Acknowledgements

This work was supported by a grant of the Romanian Ministry of Education and Research, CNCS - UEFISCDI, project number PN-III-P1-1.1-PD-2019-0894, within PNCDI III. Activities have been carried out also as part of the European Space Agency contract *Earth Observation data For Science and Innovations in the Black Sea* (EO4SIBS, ESA contract n° 4000127237/19/I-EF). In-situ data were collected using the facilities of the Sfântu Gheorghe Marine and Fluvial Research Station, University of Bucharest. We thank our colleagues, Daniel Ivanov and Ștefan Constantinescu, for their help during field campaigns. The authors would like to express their gratitude to the two anonymous reviewers who provided useful comments and suggestions.

References

Antoine, D., Morel, A., 1999. A multiple scattering algorithm for atmospheric correction of remotely sensed ocean color (MERIS instrument): principle and implementation for atmospheres carrying absorbing aerosols. Int. J. Rem. Sens. 20 (9), 1875–1916. https://doi.org/10.1080/014311699212533.

Balasubramanian, S.v., Pahlevan, N., Smith, B., Binding, C., Schalles, J., Loisel, H., Gurlin, D., Greb, S., Alikas, K., Randla, M., Bunkei, M., Moses, W., Nguyễn, H., Lehmann, M.K., O'Donnell, D., Ondrusek, M., Han, T.H., Fichot, C.G., Moore, T., Boss, E., 2020. Robust algorithm for estimating total suspended solids (TSS) in inland and nearshore coastal waters. Rem. Sens. Environ. 246 https://doi.org/10.1016/j.rse.2020.111768.

Barker, K., 2013a. In-situ measurement protocols. Part A: Apparent Optical Properties, Issue 2.0, Doc. CO-SCI-ARG-TN-0008, ARGANS Ltd., p. 126 available at: http://mermaid.acri.fr/dataproto/CO-SCI-ARG-TN-0008_In-situ_Measurement_Protocols-AOPs_Issue2_Mar2013.pdf

Barker, K., 2013b. In-situ measurement protocols. Part B: inherent optical properties and in-water constituents, issue 1.0, Doc. No: CO-SCI-ARG-TN-0008. ARGANS Ltd 39 available at: http://mermaid.acri.fr/dataproto/CO-SCI-ARG-TN-0008_In-situ_Measurement_Protocols-IOPs-Constituents_Issue1_Mar2013.pdf.

Bellacicco, M., Vellucci, V., Scardi, M., Barbieux, M., Marullo, S., D'Ortenzio, F., 2019. Quantifying the impact of linear regression model in deriving bio-optical relationships: the implications on ocean carbon estimations. Sensors 19 (13). https://doi.org/10.3390/s19133032.

Bilotta, G.S., Brazier, R.E., 2008. Understanding the influence of suspended solids on water quality and aquatic biota. Water Res. 42 (12), 2849–2861. https://doi.org/10.1016/j.watres.2008.03.018. Elsevier Ltd.

Brăescu, C.L., Zoran, M., Aiftimiei, C., Serban, F., 1997. Remote sensing methodology for coastal zones study (Black Sea). Proc. SPIE 3222, 444–455.

Brockmann, C., Doerffer, R., Peters, M., Stelzer, K., Embacher, S., Ruescas, A., 2016. Evolution of the C2RCC Neural Network for Sentinel 2 and 3 for the retrieval of ocean colour products in normal and extreme optically complex waters. In: LPS 2016 Proceedings, 1.

Constantin, S., 2022. Extreme Suspended Particulate Matter concentration events at river mouths detected by the Sentinel-3 satellite mission. Poster presentation at ESA Living Planet Symposium 23–27. May, Bonn, Germany.

Constantin, S., Doxaran, D., Constantinescu, Ștefan, 2016. Estimation of water turbidity and analysis of its spatio-temporal variability in the Danube River plume (Black Sea) using MODIS satellite data. Continent. Shelf Res. 112, 14–30. https://doi.org/10.1016/j.csr.2015.11.009.

Constantin, S., Constantinescu, Ștefan, Doxaran, D., 2017. Long-term analysis of turbidity patterns in Danube Delta coastal area based on MODIS satellite data. J. Mar. Syst. 170, 10–21. https://doi.org/10.1016/j.jmarsys.2017.01.016.

Constantinescu, A.M., Tyler, A.N., Stanica, A., Spyrakos, E., Hunter, P.D., Catianis, I., Panin, N., 2023. A century of human interventions on sediment flux variations in the Danube-Black Sea transition zone. Front. Mar. Sci. 10 https://doi.org/10.3389/fmars.2023.1068065.

Cucu-Dumitrescu, C., Constantin, S., 2017. Extraction of regions with similar temporal evolution using Earth Observation Big Data. Application to water turbidity dynamics. Remote Sensing Letters 8 (7), 627–636. https://doi.org/10.1080/2150704X.2017.1312024.

Doerffer, R., 2015. Algorithm Theoretical Bases Document (ATBD) for L2 processing of MERIS data of case 2 waters, 4th reprocessing. available online at: https://c2rcc.org/wp-content/uploads/2022/05/C2RCC_MERIS_ATBD_4Reproc_20150319.pdf.

Doerffer, R., Schiller, H., 2007. The MERIS Case 2 water algorithm. Int. J. Rem. Sens. 28 (3–4), 517–535. https://doi.org/10.1080/01431160600821127.

Dogliotti, A.I., Ruddick, K.G., Nechad, B., Doxaran, D., Knaeps, E., 2015. A single algorithm to retrieve turbidity from remotely-sensed data in all coastal and estuarine waters. Rem. Sens. Environ. 156, 157–168. https://doi.org/10.1016/j.rse.2014.09.020.

Doxaran, D., 2002. Télédetection et Modélisation Numérique Des Flux Sedimentaires Dans L'estuaire de La Gironde. PhD thesis.

Doxaran, D., Froidefond, J., Lavender, S., Castaing, P., 2002. Spectral signature of highly turbid waters Application, with SPOT data to quantify suspended particulate matter concentrations. Remote Sens. Environ. 81, 149–161.

Ducklow, H.W., Hansell, D.A., Morgan, J.A., 2007. Dissolved organic carbon and nitrogen in the western Black Sea. Mar. Chem. 105 (1–2), 140–150. https://doi.org/10.1016/j.marchem.2007.01.015.

EUMETSAT, 2021. Sentinel-3 OLCI L2 report for baseline collection OL_L2M_003. Doc. No. EUM/RSP/REP/21/1211386, available online at: https://www.eumetsat.int/media/47794.

Gohin, F., 2011. Annual cycles of chlorophyll-A, non-algal suspended particulate matter, and turbidity observed from space and in-situ in coastal waters. Ocean Sci. 7 (5), 705–732. https://doi.org/10.5194/os-7-705-2011.

Grégoire, M., Alvera-Azcaráte, A., Buga, L., Capet, A., Constantin, S., D'ortenzio, F., Doxaran, D., Faugeras, Y., Garcia-Espriu, A., Golumbeanu, M., González-Haro, C., González-Gambau, V., Kasprzyk, J.-P., Ivanov, E., Mason, E., Mateescu, R., Meulders, C., Olmedo, E., Pons, L., et al., 2023. Monitoring Black Sea environmental changes from space: new products for altimetry, ocean colour and salinity. Potentialities and requirements for a dedicated in-situ observing system. Front. Mar. Sci. 9 https://doi.org/10.3389/fmars.2022.998970.

Güttler, F.N., Niculescu, S., Gohin, F., 2013. Turbidity retrieval and monitoring of Danube Delta waters using multi-sensor optical remote sensing data: an integrated view from the delta plain lakes to the western–northwestern Black Sea coastal zone. Rem. Sens. Environ. 132, 86–101. https://doi.org/10.1016/j.rse.2013.01.009.

Han, B., Loisel, H., Vantrepotte, V., Mériaux, X., Bryère, P., Ouillon, S., Dessailly, D., Xing, Q., Zhu, J., 2016. Development of a semi-analytical algorithm for the retrieval of suspended particulate matter from remote sensing over clear to very turbid waters. Rem. Sens. 8 (3) https://doi.org/10.3390/rs8030211.

Jafar-Sidik, M., Gohin, F., Bowers, D., Howarth, J., Hull, T., 2017. The relationship between Suspended Particulate Matter and Turbidity at a mooring station in a coastal environment: consequences for satellite-derived products. Oceanologia 59 (3), 365–378. https://doi.org/10.1016/j.oceano.2017.04.003.

Karageorgis, A.P., Kourafalou, V.H., Anagnostou, C., Tsiaras, K.P., Raitsos, D.E., Papadopoulos, V., Papadopoulos, A., 2009. River-Induced particle distribution in the northwestern Black Sea (september 2002 and 2004). J. Geophys. Res. 114, 1–16. https://doi.org/10.1029/2009JC005460.

Kubryakov, A.A., Stanichny, S.v., Zatsepin, A.G., 2018. Interannual variability of Danube waters propagation in summer period of 1992–2015 and its influence on the Black Sea ecosystem. J. Mar. Syst. 179, 10–30. https://doi.org/10.1016/j.jmarsys.2017.11.001.

Kukushkin, A.S., Suslin, V.v., 2020. Assessment of applicability of satellite-derived ocean color data for studying variability of total suspended matter in the surface layer of the deep part of the Black Sea. Phys. Oceanogr. 27 (5) https://doi.org/10.22449/1573-160x-2020-5-547-556.

Margolin, A.R., Gonnelli, M., Hansell, D.A., Santinelli, C., 2018. Black Sea dissolved organic matter dynamics: insights from optical analyses. Limnol. Oceanogr. 63, 1425–1443. https://doi.org/10.1002/lno.10791.

Moore, G., Mazeran, C., Huot, J.P., 2017. Case II. S Bright pixel atmospheric correction. MERIS ATBD 2.6 (Issue 5.3).

Nazirova, K., Alferyeva, Y., Lavrova, O., Shur, Y., Soloviev, D., Bocharova, T., Strochkov, A., 2021. Comparison of in situ and remote-sensing methods to determine turbidity and concentration of suspended matter in the estuary zone of the Mzymta river, Black Sea. Rem. Sens. 13 (1), 1–29. https://doi.org/10.3390/rs13010143.

Nechad, B., Ruddick, K.G., Neukermans, G., 2009. Calibration and validation of a generic multisensor algorithm for mapping of turbidity in coastal waters. Remote Sensing of the Ocean, Sea Ice and Large Water Regions 7473. https://doi.org/10.1117/12.830700.

Nechad, B., Ruddick, K.G., Park, Y., 2010. Calibration and validation of a generic multisensor algorithm for mapping of total suspended matter in turbid waters. Rem. Sens. Environ. 114 (4), 854–866. https://doi.org/10.1016/j.rse.2009.11.022.

Nechad, B., Dogliotti, A., Ruddick, K.G., Doxaran, D., 2016. Particulate backscattering retrieval from remotely-sensed turbidity in various coastal and riverine turbid waters. Proceedings of ESA Living Planet Symposium. Prague, 9-13 May 2016, ESA-SP 740.

Neukermans, G., Ruddick, K., Loisel, H., Roose, P., 2012. Optimization and quality control of suspended particulate matter concentration measurement using turbidity measurements. Limnol Oceanogr. Methods 10, 1011–1023. https://doi.org/10.4319/lom.2012.10.1011.

Novoa, S., Doxaran, D., Ody, A., Vanhellemont, Q., Lafon, V., Lubac, B., Gernez, P., 2017. Atmospheric corrections and multi-conditional algorithm for multi-sensor remote sensing of suspended particulate matter in low-to-high turbidity levels coastal waters. Rem. Sens. 9 (1) https://doi.org/10.3390/rs9010061.

Ody, A., Doxaran, D., Vanhellemont, Q., Nechad, B., Novoa, S., Many, G., Bourrin, F., Verney, R., Pairaud, I., Gentili, B., 2016. Potential of high spatial and temporal ocean color satellite data to study the dynamics of suspended particles in a micro-tidal River plume. Rem. Sens. 8 (3), 245. https://doi.org/10.3390/rs8030245.

Pahlevan, N., Mangin, A., Balasubramanian, S.V., Smith, B., Alikas, K., Arai, K., Barbosa, C., Bélanger, S., Binding, C., Bresciani, M., Giardino, C., Gurlin, D., Fan, Y., Harmel, T., Hunter, P., Ishikaza, J., Kratzer, S., Lehmann, M.K., Ligi, M., Ma, R., Martin-Lauzer, F.R., Olmanson, L., Oppelt, N., Pan, Y., Peters, S., Reynaud, N., Sander de Carvalho, L.A., Simis, S., Spyrakos, E., Steinmetz, F., Stelzer, K., Sterckx, S., Tormos, T., Tyler, A., Vanhellemont, Q., Warren, M., 2021. ACIX-Aqua: a global assessment of atmospheric correction methods for Landsat-8 and Sentinel-2 over lakes, rivers, and coastal waters. Rem. Sens. Environ. 258, 112366 https://doi.org/10.1016/j.rse.2021.112366.

Preoteasa, L., Vespremeanu-Stroe, A., Tătui, F., Zăinescu, F., Timar-Gabor, A., Cîrdan, I., 2016. The evolution of an asymmetric deltaic lobe (Sf. Gheorghe, Danube) in association with cyclic development of the river-mouth bar: long-term pattern and present adaptations to human-induced sediment depletion. Geomorphology 253 (November), 59–73. https://doi.org/10.1016/j.geomorph.2015.09.023.

Sorokin, YuI., 1983. The Black Sea. In: Ketchum, B.H. (Ed.), Estuaries and Enclosed Seas. Ecosystems of the World. Elsevier, Amsterdam, pp. 253–292.

Stanev, E.V., Kandilarov, R., 2012. Sediment dynamics in the Black Sea: numerical modelling and remote sensing observations. Ocean Dynam. 62 (4), 533–553. https://doi.org/10.1007/s10236-012-0520-1.

Stramski, D., Constantin, S., Reynolds, R.A., 2023. Adaptive optical algorithms with differentiation of water bodies based on varying composition of suspended particulate matter: A case study for estimating the particulate organic carbon concentration in the western Arctic seas. Rem. Sens. Environ. 286. https://doi.org/10.1016/j.rse.2022.113360.

Tavora, J., Boss, E., Doxaran, D., Hill, P., 2020. An algorithm to estimate suspended particulate matter concentrations and associated uncertainties from remote sensing reflectance in coastal environments. Rem. Sens. 12 (13) https://doi.org/10.3390/rs12132172.

Valente, A., Sathyendranath, S., Brotas, V., Groom, S., Grant, M., Jackson, T., Chuprin, A., Taberner, M., Airs, R., Antoine, D., Arnone, R., Balch, W.M., Barker, K., Barlow, R., Bélanger, S., Berthon, J.-F., Beşiktepe, Ş., Borsheim, Y., Bracher, A., Brando, V., Brewin, R.J.W., Canuti, E., Chavez, F.P., Cianca, A., Claustre, H., Clementson, L., Crout, R., Ferreira, A., Freeman, S., Frouin, R., García-Soto, C., Gibb, S.W., Goericke, R., Gould, R., Guillocheau, N., Hooker, S.B., Hu, C., Kahru, M., Kampel, M., Klein, H., Kratzer, S., Kudela, R., Ledesma, J., Lohrenz, S., Loisel, H., Mannino, A., Martinez-Vicente, V., Matrai, P., McKee, D., Mitchell, B.G., Moisan, T., Montes, E., Muller-Karger, F., Neeley, A., Novak, M., O'Dowd, L., Ondrusek, M., Platt, T., Poulton, A.J., Repecaud, M., Röttgers, R., Schroeder, T., Smyth, T., Smythe-Wright, D., Sosik, H.M., Thomas, C., Thomas, R., Tilstone, G., Tracana, A., Twardowski, M., Vellucci, V., Voss, K., Werdell, J., Wernand, M., Wojtasiewicz, B., Wright, S., Zibordi, G., 2022. A compilation of global bio-optical in situ data for ocean-colour satellite applications – version three. Earth Syst. Sci. Data Discuss. https://doi.org/10.5194/essd-2022-159 [preprint].

Van der Zande, D., Stelzer, K., Lebreton, C., Dille, A., Shevchuk, R., Santos, J., Böttcher, M., Vanhellemont, Q., Scholze, J., 2022. Copernicus marine Service. Available online at: Quality Information Document - OCEANCOLOUR_*_BGC_HR_*_*_009_201to212 https://catalogue.marine.copernicus.eu/documents/QUID/CMEMS-HR-OC-QUID-009-201to212.pdf.

Wei, J., Wang, M., Jiang, L., Yu, X., Mikelsons, K., Shen, F., 2021. Global estimation of suspended particulate matter from satellite ocean color imagery. J. Geophys. Res.: Oceans 126 (8). https://doi.org/10.1029/2021jc017303.

Yu, X., Lee, Z.P., Shen, F., Wang, M., Wei, J., Jiang, L., Shang, Z., 2019. An empirical algorithm to seamlessly retrieve the concentration of suspended particulate matter from water color across ocean to turbid river mouths. Rem. Sens. Environ. 235, 111491 https://doi.org/10.1016/j.rse.2019.111491.

Zăinescu, F., Vespremeanu-Stroe, A., Anthony, E., Tătui, F., Preoteasa, L., Mateescu, R., 2019. Flood deposition and storm removal of sediments in front of a deltaic wave-influenced river mouth. Mar. Geol. 417 https://doi.org/10.1016/j.margeo.2019.106015.

Zibordi, G., Berthon, J.F., Doyle, J.P., Grossi, S., van der Linde, D., Targa, C., Alberotanza, L., 2002. Coastal atmosphere and sea time series (CoASTS), Part 1: along-term measurement program. In: Hooker, S.B., Firestone, E.R. (Eds.), NASA Tech. Memo. 2002-206892, 19. NASA Goddard Space Flight Center, Greenbelt, MD.

Zibordi, G., Berthon, J.-F., Canuti, E., 2011. Cross-site consistent in situ measurements for satellite ocean color applications: the BiOMaP radiometric dataset. Rem. Sens. Environ. 115, 2104–2115. https://doi.org/10.1016/j.rse.2011.04.013.